Training and projecting: A reduced basis method emulator for many-body physics

Edgard Bonilla [1,*,†], Pablo Giuliani [2,3,*,‡], Kyle Godbey [2,§], and Dean Lee [2,4,‖]

[1] *Department of Physics, Stanford University, Stanford, California 94305, USA*
[2] *Facility for Rare Isotope Beams, Michigan State University, East Lansing, Michigan 48824, USA*
[3] *Department of Statistics and Probability, Michigan State University, East Lansing, Michigan 48824, USA*
[4] *Department of Physics and Astronomy, Michigan State University, East Lansing, Michigan 48824, USA*

(Received 18 March 2022; revised 14 May 2022; accepted 25 October 2022; published 17 November 2022)

We present the reduced basis method as a tool for developing emulators for equations with tunable parameters within the context of the nuclear many-body problem. The method uses a basis expansion informed by a set of solutions for a few values of the model parameters and then projects the equations over a well-chosen low-dimensional subspace. We connect some of the results in the eigenvector continuation literature to the formalism of reduced basis methods and show how these methods can be applied to a broad set of problems. As we illustrate, the possible success of the formalism on such problems can be diagnosed beforehand by a principal component analysis. We apply the reduced basis method to the one-dimensional Gross-Pitaevskii equation with a harmonic trapping potential and to nuclear density functional theory for ^{48}Ca, achieving speed-ups of more than $\times 150$ and $\times 250$, respectively, when compared to traditional solvers. The outstanding performance of the approach, together with its straightforward implementation, show promise for its application to the emulation of computationally demanding calculations, including uncertainty quantification.

DOI: 10.1103/PhysRevC.106.054322

I. INTRODUCTION

Most modern theoretical models describing many-body nuclear dynamics share an ever-increasing computational burden. This can turn into a challenge for tasks like uncertainty quantification analysis [1,2], experimental design [3,4], calibration of model parameters [5–7], and repeated evaluation for different inputs [8,9]. Emulators—algorithms capable of providing fast yet accurate approximations to expensive computations—have been gaining increasing importance as a way to circumvent these challenges [1,10].

In recent years, a technique called eigenvector continuation [11] was developed to emulate computationally intensive calculations involving bound states of Hamiltonian operators [12] and nuclear scattering [13–15]. Eigenvector continuation has shown excellent performance in interpolation and extrapolation by working with two elements: choosing its ansatz functions from the linear span of exact solutions to the problem at hand, and using a variational principle—for example, the Rayleigh-Ritz method [11,16] or the Kohn variational principle [13,17]—to obtain equations for the coefficients of this linear combination.

In this article, we present an emulator constructed in the formalism of reduced basis methods (RBMs) [18–20], a set of dimensionality-reduction techniques that fall under the umbrella of reduced-order models [21–23]. These methods have seen active development over the last two decades, proving to be useful in a variety of computationally intensive problems involving partial differential equations [24–27]. As we show in the discussion, the eigenvector continuation technique is naturally connected to RBMs when the former is generalized through a Galerkin method formulation. The key insight is that once a reasonable choice of ansatz functions has been made (for example, the basis of exact solutions used in eigenvector continuation), all that is needed is a method to select a suitable candidate approximation from the ansatz subspace. This could be achieved, for instance, by using a variational principle, minimizing a cost functional, or by finding the fixed point of an iterative scheme. Among the alternatives, the Galerkin method—the option chosen in RBMs—stands out for its simplicity: it attempts to find an accurate approximate solution by projecting the problem to a well-chosen very-low dimensional subspace. This simplicity allows these methods to be applied to a wide variety of problems in a straightforward way, including nonlinear coupled differential equations. Although common in the many-body physics context, these nonlinear problems have not yet been explored in the eigenvector continuation literature.

We structure the rest of the article as follows. In Sec. II, we explain the formalism of RBMs, highlighting their connection with established results on the literature of eigenvector continuation, as well as showing how the Galerkin formulation extends their application to coupled equations and nonlinear problems. Additionally, Sec. II illustrates the use of the principal component analysis as a diagnostic tool for the success of

*These authors contributed equally to this work.
†edgard@stanford.edu
‡giulianp@frib.msu.edu
§godbey@frib.msu.edu
‖leed@frib.msu.edu

reduced basis emulators on specific problems. In Sec. III we demonstrate the effectiveness of the method by constructing emulators for two nonlinear problems, the ground state of the Gross-Pitaevskii equation with a harmonic trapping potential, and the ground state of ^{48}Ca using the Skyrme effective interaction. We conclude our discussion by highlighting the potential role that these emulation techniques could have in the future of uncertainty quantification in nuclear physics.

II. THE REDUCED BASIS METHOD FRAMEWORK

RBMs are tailored to problems that feature an equation that depends smoothly on a list of tunable control parameters α [19]. The goal is to build an approximate solution for a suitable range of these parameters. Let us assume the equation is written in the general form

$$F_\alpha(\phi_\alpha) = 0, \tag{1}$$

where ϕ_α is a vector (or function) from a Hilbert space $\mathcal{H}$, and F_α maps $\mathcal{H}$ onto itself. For example, in the case of bound systems with a Hamiltonian H_α that depends on the parameters α, F_α can take the form of the eigenvalue equation $F_\alpha(\phi_\alpha) = H_\alpha\phi_\alpha - \lambda_\alpha\phi_\alpha$, where λ_α is the eigenvalue. Another example would be the case of single-channel scattering where F_α can be the radial part of the scattering equation [28] $F_\alpha(\phi_\alpha) = (-\frac{d^2}{dr^2} + \frac{\ell(\ell+1)}{r^2} + U(r,\alpha) - p^2)\phi_\alpha(r)$, where a system with reduced mass μ interacts through a potential $V(r,\alpha) = U(r,\alpha)/2\mu$ with parameters α, ℓ is the angular momentum quantum number, and p is the asymptotic linear momentum. The RBM finds approximate solutions $\hat{\phi}_\alpha$ to these—and more general—problems by constructing a basis expansion with n linearly independent "reduced basis" functions $\{\phi_k\}_{k=1}^n$:

$$\hat{\phi}_\alpha = \phi_0 + \sum_{k=1}^{n} a_k\phi_k, \tag{2}$$

where the coefficients a_k of the approximation will depend on the specific values of α, but the basis functions ϕ_k will not. ϕ_0 is an extra term that can be added to satisfy boundary conditions imposed on Eq. (1). The reduced basis functions ϕ_k are selected to create an affine space (the ansatz subspace) *close* to the manifold formed by the solutions to Eq. (1) as a function of the parameters α [19] by using the information from a (possibly small) sample of exact solutions. In practice, the "exact solutions" (or "snapshots") of Eq. (1) are constructed by highly accurate yet computationally expensive approximations such as finite element or spectral calculations [24].

One way to build the reduced basis for Eq. (2) is the approach taken in many eigenvector continuation applications [11–15], also known as the Lagrange basis [24]. It consists of calculating n "training functions" $\{\tilde{\phi}_k\}_{k=1}^n$ as solutions to Eq. (1) for n values α_k $[F_{\alpha_k}(\tilde{\phi}_k) = 0]$ and then choosing the reduced basis as these n training functions $\phi_k = \tilde{\phi}_k$. One possible way to improve upon this choice is the so-called proper orthogonal decomposition (POD) [19]. It consists of computing $N \geqslant n$ solutions $\{\tilde{\phi}_l\}_{l=1}^N$ and constructing the reduced basis with the first n components from a principal component analysis (PCA) [29], or singular value decomposition (SVD) [30], of the set of these N training functions. Therefore, by using the information of N samples, the POD basis is more robust than a Lagrange basis of dimension n and faster than a Lagrange basis of N training points.

Once the n reduced basis functions are chosen, the coefficients a_k for the approximation are found by the Galerkin method [31], that is, by projecting Eq. (1) over n linearly independent "projecting functions" $\{\psi_j\}_{j=1}^n$ in the Hilbert space:

$$\langle\psi_j|F_\alpha(\hat{\phi}_\alpha)\rangle = 0, \quad \text{for all } j. \tag{3}$$

$F_\alpha(\hat{\phi}_\alpha)$ is often called the residual [32], and it can be used, for example, to inform the construction of the reduced basis [33], or to estimate the emulation error [34]. We can interpret Eqs. (3) as enforcing the orthogonality of $F_\alpha(\hat{\phi}_\alpha)$ to the subspace spanned by $\{\psi_j\}_{j=1}^n$, i.e., by finding a $\hat{\phi}_\alpha$ such that $F_\alpha(\hat{\phi}_\alpha)$ is "zero" up to the ability of the set $\{\psi_j\}_{j=1}^n$. The choice of projecting functions ψ_j is arbitrary, but is usually also informed by the solution manifold [19,20]. For the rest of this work, we choose ψ_j to enforce orthogonality with respect to the ansatz subspace (2), which is the traditional way of using the Galerkin method [32].

The reduced-basis emulators are most effective, in terms of speed-ups, when the projections in Eqs. (3) lead, for every j, to expressions of the form

$$\sum_{m=1}^{M_j} f_{j,m}(\alpha)g_{j,m}(a_1,\ldots,a_n) = 0, \tag{4}$$

where $f_{j,m}(\alpha)$ and $g_{j,m}(a_1,\ldots,a_n)$ are M_j functions that are independent of the intrinsic coordinates of the original system. If these functions can be computed only once and then stored in memory, we can avoid performing costly integrals or finite element calculations every time we have to solve Eqs. (3) for a new set of parameters α. This property is exploited later when we construct an emulator for the Gross-Pitaevskii equation in Eq. (14).

A. Connections to the eigenvector continuation literature

To illustrate the application of the RBM and connect with previous results in the eigenvector continuation literature, we work with the bound system eigenvalue equation and the radial scattering equation, the two formerly mentioned examples for F_α. As already mentioned, for the single-channel scattering example, Eq. (1) takes the following form:

$$F_\alpha(\phi) = \left(-\frac{d^2}{dr^2} + \frac{\ell(\ell+1)}{r^2} + U(r,\alpha) - p^2\right)\phi(r) = 0. \tag{5}$$

Following Ref. [13], let us assume that the solution to this equation is subject to the boundary conditions $\phi(r=0) = 0$, and

$$\phi(r) \underset{r\to\infty}{\longrightarrow} \frac{1}{p}\sin\left(pr - \ell\frac{\pi}{2}\right) + \tau\cos\left(pr - \ell\frac{\pi}{2}\right). \tag{6}$$

Note that Eq. (6) imposes a normalization condition on ϕ: the coefficient accompanying the sine function must equal $1/p$.

A straightforward application of the RBM with a Lagrange basis of size n leads to the choice of an approximate function:

$$\hat{\phi}_\alpha = \sum_{k=1}^{n} a_k \phi_k, \quad \text{with} \quad \sum_{k=1}^{n} a_k = 1, \tag{7}$$

where the ϕ_k are solutions to $F_{\alpha_k}(\phi_k) = 0$ with the correct boundary conditions. We can eliminate the redundancy of the coefficients a_k created by the boundary conditions by explicitly writing one of the them in terms of the others. Without loss of generality, we let $a_1 = 1 - \sum_{k=2}^{n} a_k$, obtaining

$$\hat{\phi}_\alpha = \phi_1 + \sum_{k=2}^{n} a_k(\phi_k - \phi_1). \tag{8}$$

We can identify $(\phi_k - \phi_1)$ for $k \geqslant 2$ as the relevant elements in the basis expansion and select $\psi_k = (\phi_k - \phi_1)$ as the associated projecting functions, leading to the following equations:

$$\sum_{k=1}^{n} a_k \langle \phi_j - \phi_1 | F_\alpha(\phi_k) \rangle = 0, \quad \text{for} \quad 2 \leqslant j \leqslant n. \tag{9}$$

These equations—formulated from a geometric projection argument—are equivalent to those obtained by the Kohn variational principle [35], as done in Refs. [13,15]. The proof is elaborated in Appendix A.

In the bound system example, with $\psi_k = \phi_k$, Eqs. (3) might not have a solution for the exact eigenvalue. Allowing λ_α to be approximated by $\hat{\lambda}_\alpha$ helps ensure we can solve the projected equations:

$$\sum_{k=1}^{n} a_k \langle \phi_j | H_\alpha | \phi_k \rangle = \hat{\lambda}_\alpha \sum_{k=1}^{n} a_k \langle \phi_j | \phi_k \rangle, \quad \text{for all } j, \tag{10}$$

where the set a_k and the approximate eigenvalue $\hat{\lambda}_k$ add up to $(n+1)$ unknowns. We can complete the set of equations with a normalization condition: $\langle \hat{\phi}_\alpha | \hat{\phi}_\alpha \rangle = 1$. When choosing ϕ_k as exact solutions for different α, Eq. (10) is equivalent to the generalized eigensystem formulated with the Rayleigh-Ritz variational method from the eigenvector continuation approach [11].

Beyond these two examples, the generality of the Galerkin formalism allows to apply RBMs to a wide variety of problems, including discrete, operator, integral, and differential equations [32,36]. For instance, the projected equations (3) can be directly applied to nonlinear problems like nonlinear eigenvalue equations where $F_\alpha(\phi_\alpha) = G_\alpha(\phi_\alpha) - \lambda_\alpha \phi_\alpha$, with G_α being a general operator. As such, we can consider the RBM a natural extension of the eigenvector continuation technique with a broader range of applicability.

Additionally, the RBM can be applied to the case of a set of m coupled equations—common in many-body physics—by letting

$$F_\alpha^{(i)}\left(\phi_\alpha^{(1)}, \ldots, \phi_\alpha^{(m)}\right) = 0, \quad \text{for} \quad i = 1, \ldots, m, \tag{11}$$

represent the set of equations and by approximating each coupled function $\phi_\alpha^{(i)}$ as a linear combination of their corresponding solutions for different values of α:

$$\hat{\phi}_\alpha^{(i)} = \phi_0^{(i)} + \sum_{k=1}^{n_i} a_k^{(i)} \phi_k^{(i)}, \quad \text{for} \quad k = 1, \ldots, n_i; \;\; i = 1, \ldots, m. \tag{12}$$

We can then select $\psi_j^{(i)}$ as the generators of the affine spaces for each $\hat{\phi}_\alpha^{(i)}$, to obtain a total of $n_{\text{Tot}} = \sum_{i=1}^{m} n_i$ Galerkin equations:

$$\left\langle \psi_j^{(i)} \middle| F_\alpha^{(i)}\left(\phi_\alpha^{(1)}, \ldots, \phi_\alpha^{(m)}\right) \right\rangle = 0, \tag{13}$$

for $j = 1, \ldots, n_i$, and $i = 1, \ldots, m$, which can be solved for the n_{Tot} coefficients $a_k^{(i)}$.

In the case of coupled eigenvalue-eigenvector systems, we can proceed as in the case of a single equation, by substituting the m eigenvalues $\lambda_\alpha^{(i)}$ for approximate values $\hat{\lambda}_\alpha^{(i)}$ and enforcing m normalization conditions, in accordance with the requirements of the problem at hand.

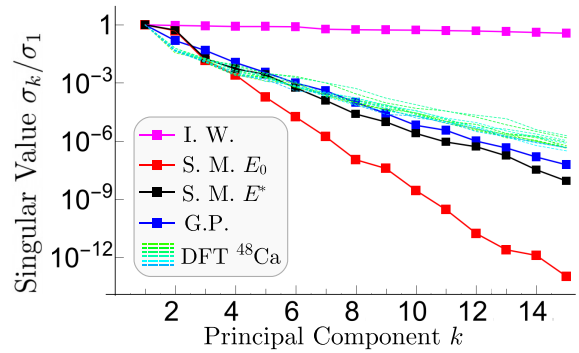

FIG. 1. Decay of the singular values σ_k for a set of solutions of the infinite well (I.W. in magenta), the single channel two-body scattering with a Minnesota potential [37] with fixed energy (S.M. $E_0 = 50$ MeV in red) and varying energy (S.M. $E^* \in [20, 80]$ MeV in black) with the parameter's range as used in Ref. [13], the Gross-Pitaevskii equation (G.P. in blue), and the solutions for the 13 energy levels in ^{48}Ca (DFT in dashed green-blue lines). Appendix B contains additional details on these calculations, including the ranges for the values of α used.

B. Testing for low-dimensionality with principal component analysis (PCA)

It is important to note that if the solution manifold ϕ_α for the problem at hand cannot be sufficiently embedded in a *linear* subspace, then the RBM we described will not constitute an effective emulator. In practice, to test whether a problem is fit for emulation via RBMs, it is sufficient to observe the decay of the singular values σ_k associated with the PCA of a group of exact solutions $\tilde{\phi}_\alpha$ for various α [19]. An exponential decay on the associated singular values σ_k from the PCA indicates that the RBM can provide an accurate approximation for the given problem [19,24,38]. As such, it is good practice to use the PCA of a set of solutions as an *a priori* test for the success of the RBM emulator.

This exact diagnosis is showcased in Fig. 1, which shows the singular values σ_k for the problems discussed in our work.

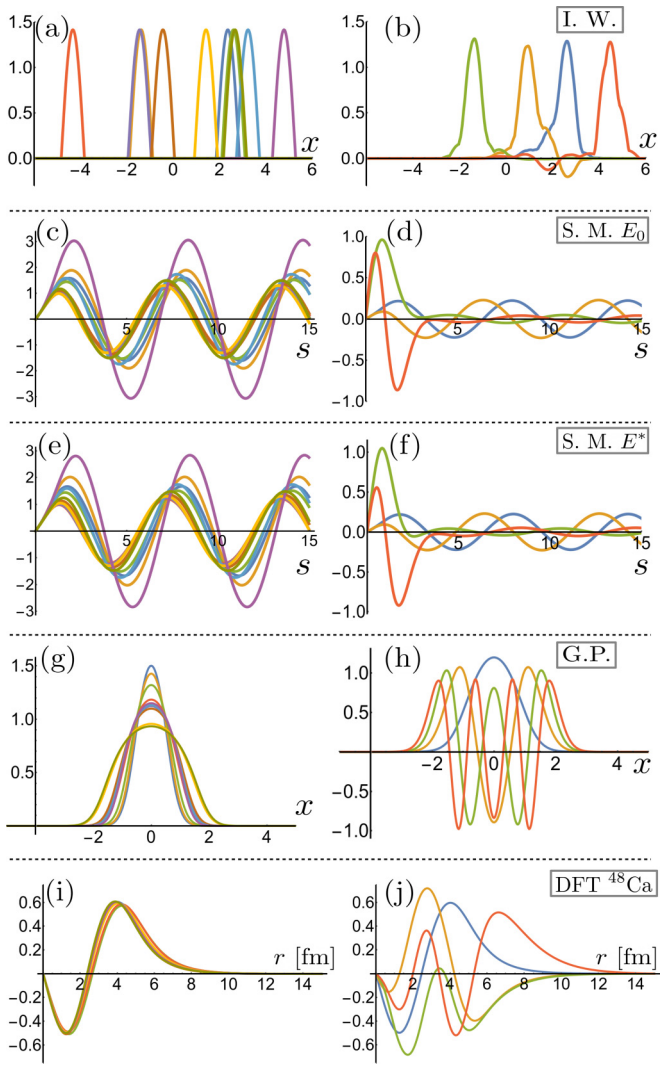

FIG. 2. Examples of 10 solutions (left column) and the first four principal components out of more than 40 exact solutions (right column) for the problems shown in Fig. 1. Panels (a) and (b) correspond to the infinite well; panels (c) and (d) to the scattering with the Minnesota potential at a fixed energy; panels (e) and (f) to the scattering with the Minnesota potential with a variable energy; panels (g) and (h) to the Gross-Pitaevskii equation; and panels (i) and (j) to ^{48}Ca under DFT. For panels (i) and (j) we chose the $^2S_{1/2}$ neutron wave function as a showcase, out of the total of 13 distinct levels for protons and neutrons.

We included a counterexample to illustrate a situation where the RBM would fail to create a good surrogate model. A sample of the corresponding exact solutions $\tilde{\phi}_\alpha$ and principal vectors are shown in Fig. 2.

First, we analyze the scattering wave functions in the $^1S_0$ channel at a fixed energy [Eq. (5) with $\ell = 0$] for the Minnesota potential [37]: $U(r, V_{0R}, V_{0S}) = 2\mu(V_{0R}e^{-1.487r^2} + V_{0S}e^{-0.465r^2})$. For this example, $\alpha = \{V_{0R}, V_{0S}\}$. The rapid exponential decay of the σ_k in Fig. 1 is consistent with the excellent results obtained in Ref. [13]. A similar pattern is obtained for wave functions across energies (black squares in Fig. 1) by rescaling the scattering differential equation (5) via the change of variable $s = pr$. This change makes all exact solutions $\tilde{\phi}_\alpha(s)$ share the same asymptotic behavior. The parameter list $\alpha = \{V_{0R}, V_{0S}, E = p^2/2\mu\}$ now includes the varying energy. The exponential decay of σ_k implies that it should be possible to build a scattering emulator across energies, which could be a useful upgrade to the emulators showcased in Refs. [13,15].

Next, we analyze the example constructed with the 1D quantum Hamiltonian of a particle trapped in an infinite well [39] by letting α control the location of the well: $V(x, \alpha) = 0$ for $x \in [\alpha, \alpha + 1]$ and $V(x, \alpha) = \infty$ otherwise. As shown in Fig 1, a direct application of the RBM fails to accurately emulate the ground-state wave function as α changes. Figure 2(a) shows the ground-state wave functions for a sample of well locations α, making it evident that a linear combination of a few exact solutions will not be sufficient to represent the ground-state variation as a function of α. This intuition is reflected by the slow decay of σ_k in Fig. 1. Extensions to the basic methodology can tackle these issues by allowing further manipulation of the reduced basis (see, for example, Ref. [38]). In this particular case, taking advantage of the symmetry of the problem with a translation, i.e., $\phi_\alpha(x + \alpha) = \phi_{\alpha=0}(x)$, would lead to all σ_k's being zero for $k \geqslant 2$.

The final two examples in Figs. 1 and 2 are the Gross-Pitaevskii equation and the 13 energy levels of ^{48}Ca under density functional theory (DFT). The decay of their respective σ_k's also makes them excellent candidates for the application of the RBM, as we explore next.

III. EMULATING NONLINEAR SYSTEMS

A. The Gross-Pitaevskii equation

The Gross-Pitaevskii equation [40,41] (see also Ref. [42] for a RBM application) is a nonlinear Schrödinger equation that approximately describes the low-energy properties of dilute Bose-Einstein condensates. Using a self-consistent mean-field approximation, the many-body wave function is reduced to a description in terms of a single complex-valued wave function $\phi(\vec{r})$. We work with the one-dimensional Gross-Pitaevskii equation [43–46] with a harmonic trapping potential by letting F_α be

$$F_{q,\kappa}(\phi) = -\phi'' + \kappa x^2\phi + q|\phi|^2\phi - \lambda_{q,\kappa}\phi = 0, \qquad (14)$$

where κ, q, and $\lambda_{q,\kappa}$ are proportional to the strength of the harmonic trapping, the self-coupling of the wave function, and the ground-state energy, respectively. $\phi(x)$ is a single variable function that depends on x and it is normalized to unity. Note that, since this equation depends linearly on κ and q, the projection equations (3) that involve integrals in x can be evaluated and stored for faster computation, leading to expressions of the form shown in Eq. (4). For example, the term associated with the harmonic trapping reads

$$\langle\psi_j|\kappa x^2|\hat{\phi}\rangle = \sum_{k=1}^{n} a_k\kappa \int \psi_j(x)x^2\phi_k(x)dx. \qquad (15)$$

To test the RBM for extrapolation, we built a Lagrange basis with four training functions $\tilde{\phi}_i$ in the $[q, \kappa]$ space as

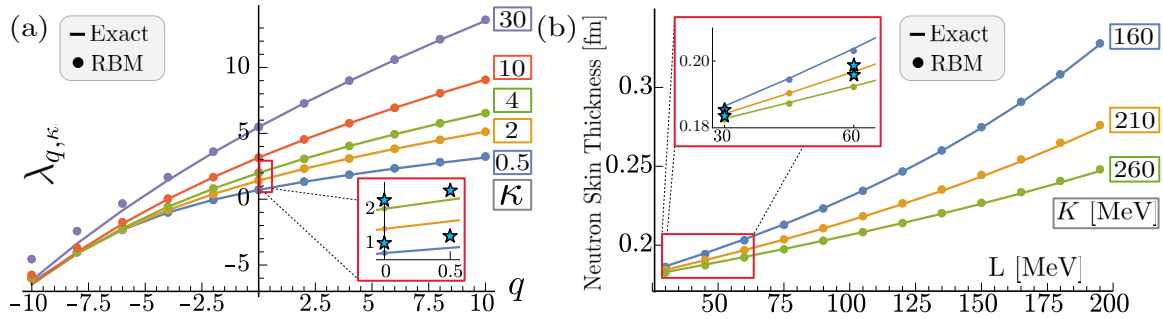

FIG. 3. Comparison between the exact solvers (solid lines) and the RBM (solid circles) calculations. Panel (a) shows the ground-state energy $\lambda_{q,\kappa}$ of the Gross-Pitaevskii equation as a function of q for the values of $\kappa = 0.5$, 2, 4, 10, and 30. Panel (b) shows the neutron skin thickness of ^{48}Ca as a function of L for the values of $K = 160$, 210, and 260 MeV. In both figures, the Lagrange basis with four points is shown as cyan stars within the inset plots. Appendix B contains additional details on these calculations.

exact solutions $[F_{q_i,\kappa_i}(\tilde{\phi}_i) = 0]$, with the projecting functions as $\psi_i = \phi_i$. Figure 3(a) shows the results of emulating $\lambda_{q,\kappa}$ by using this basis and applying Eqs. (3) plus the normalization condition. The agreement between the exact and emulated calculations is excellent, with an error of less than 2.5% in the repulsive phase ($q \geqslant 0$) where the four training parameters are located, and it deteriorates only in the attractive phase ($q < 0$) well beyond the training region. In contrast with the original implementations of eigenvector continuation [11], extrapolation is not a feature usually exploited on the RBM literature. Making full use of the techniques developed in the RBM literature could nonetheless be key when calculations of exact solutions in a specific phase of the system are numerically unstable or impossible, but approximable by such methods.

In addition to extrapolating, we explored a situation similar to how emulators are tested for uncertainty quantification [12,15]. Using a Latin hypercube sampling (LHS) [47], we drew 500 testing points in the range $q \in [0, 30]$ and $\kappa \in [5, 30]$. We constructed three types of reduced basis: Lagrange, POD, and POD + Greedy, each with three sizes $n = 2$, 4, and 8. The Lagrange basis consisted of n exact solutions drawn with LHS. The POD and POD + Greedy consisted of n principal components from a set of $N = 20$ exact solutions. For the POD the N exact solutions were drawn using LHS, while for the POD + Greedy the first solution was placed at a central location and the other $N - 1$ were included one-by-one through a Greedy algorithm inspired on Refs. [48–50]. Our Greedy approach finds the parameter set $[q_{m+1}, \kappa_{m+1}]$ for the next exact solution $\tilde{\phi}_{m+1}$, by maximizing the norm of the residual $F_{q,\kappa}(\hat{\phi}_{q,\kappa})$ over a LHS of parameters $[q, \kappa]$. In each step, $\hat{\phi}_{q,\kappa}$ is constructed with a POD basis informed by the previous m exact solutions.

Table I shows the relative root-mean-squared errors, which converge exponentially as more bases are added, as expected from the results shown in Fig. 1. Both POD bases were more accurate and robust than the Lagrange basis, which produced results that frequently changed by more than an order of magnitude when resampling the exact solutions for the basis. For $n = 8$ the accuracy of the POD + Greedy basis was more than 600 times better than the Lagrange basis. In terms of speed-up when calculating the 500 testing points, the three reduced bases with $n = 2$ were almost 150 times faster than the exact solver, while $n = 4$ and $n = 8$ obtained speed-ups of 40 and 5 times, respectively.

B. Skyrme density functional theory

We now proceed to use the RBM in realistic nuclear DFT calculations. DFT is a widely applied microscopic formalism [51] (see also Refs. [52–54] for other RBM applications to DFT). In nuclear physics it is used to describe properties of nuclei from the mean-field perspective; i.e., each nucleon interacts with an average effective field made up of all the particles in the system. This interaction is then constructed in a self-consistent way: the wave function of each nucleon and its eigenenergy are found at the same time as the effective field they produce and interact with. As such, the Hamiltonian $\hat{h}^{(i)}$ acting on the ith wave function $\phi^{(i)}$ depends on all M of them:

$$\hat{h}^{(i)}[\Phi]\phi^{(i)} - \lambda^{(i)}\phi^{(i)} = 0 \quad \text{for} \quad 1 \leqslant i \leqslant M, \tag{16}$$

where $\Phi = \{\phi^{(i)}\}_{i=1}^{M}$, and the parameter list α has been omitted for the sake of clarity. The dependence of the Hamiltonian on the wave functions comes from, for example, the total nuclear density ρ and the kinetic energy density τ. We derive the single-particle Hamiltonian $\hat{h}^{(i)}$ from the Skyrme effective

TABLE I. Root-mean-squared errors for the Gross-Pitaevskii and DFT problems described in the text. The errors are defined as $\langle[(A_{\text{RBM}} - A_{\text{exact}})/A_{\text{exact}}]^2\rangle^{1/2}$, where A is the quantity being computed and $\langle\rangle$ denotes average. Three cases of the reduced basis size were explored with $n = 2$, 4, and 8. Five hundred testing points were drawn in their respective parameter space, but for DFT 32 points were excluded from the statistics since the exact solver reported convergence problems. Appendix B contains additional details on these calculations.

Basis	Gross-Pitaevskii ground-state energy			^{48}Ca average particle energy
n	Lagrange	POD	POD Greedy	POD
2	1.0×10^{-1}	1.2×10^{-2}	1.5×10^{-2}	5.9×10^{-3}
4	3.0×10^{-3}	5.6×10^{-4}	2.1×10^{-4}	6.1×10^{-4}
8	1.3×10^{-5}	1.2×10^{-6}	2.0×10^{-8}	1.7×10^{-4}

interaction [55–58], the nuclear part of which can be written as a general energy density functional (EDF) of time-even densities [59]:

$$\begin{aligned}\mathcal{H}_t(r) = C_t^{\rho}\rho_t^2 + C_t^{\rho\Delta\rho}\rho_t\Delta\rho_t + C_t^{\tau}\rho_t\tau_t \\ + C_t^{J}\overleftrightarrow{J}_t^2 + C_t^{\rho\nabla J}\rho_t\nabla\cdot\mathbf{J}_t,\end{aligned} \tag{17}$$

where the subscript $t = (0, 1)$ represents isoscalar and isovector densities, respectively. The parameters of this EDF, C_t^{τ} for instance, model the coupling between the particles and the nucleonic density in question (the kinetic energy density τ in this case). As it is usually done in modern EDF optimization [60,61], we can parametrize those couplings in terms of nuclear-matter properties plus the remaining coupling constants left unconstrained:

$$\left\{\rho_c, E^{\mathrm{NM}}/A, K^{\mathrm{NM}}, a_{\mathrm{sym}}^{\mathrm{NM}}, L_{\mathrm{sym}}^{\mathrm{NM}}, M_s^*, C_t^{\rho\Delta\rho}, C_t^{\rho\nabla J}\right\}. \tag{18}$$

This representation is primarily rooted in physical observables—like the nuclear saturation density ρ_c—and simplifies the selection of a sensible range of values to explore in model calibration for DFT and for constructing the training bases for the RBM.

To test the RBM in extrapolation for DFT, we built a Lagrange basis of four points spanning $L_{\mathrm{sym}}^{\mathrm{NM}} = 30$ and 60 MeV and $K^{\mathrm{NM}} = 200$ and 220 MeV while the other parameters remained at their optimized UNEDF1 values [62]. The wave functions on each shell (seven for neutrons and six for protons) were calculated using both the exact solver and the RBM emulator. Figure 3(b) shows the performance of the emulator when calculating the neutron skin thickness of ^{48}Ca [63], a quantity particularly sensitive to the $L_{\mathrm{sym}}^{\mathrm{NM}}$ parameter. The agreement between the emulated values and exact DFT results is excellent, with an error of less than 0.8% for all extrapolated values shown, even for $L_{\mathrm{sym}}^{\mathrm{NM}}$ and K^{NM} well outside the training zone.

To test the limits of the emulator, the range of all ten available parameters in Eq. (18) were widened well beyond what is reasonable for realistic nuclear matter. We used LHS to draw 50 training points to build a POD basis with $n = 2$, 4, and 8 and to independently draw 500 testing points within the widened parameter ranges. As such, several parameter combinations yielded convergence issues for the DFT solver, but not for the emulated calculations, highlighting the capability of RBMs to extrapolate into regions where exact solvers can experience numerical instabilities. Even though the emulated results of nonconverging test points seemed reasonable, we consider their validation to be beyond the scope of this work.

As Table I shows, for the stable parameter sets, the RBM reproduces single nucleon energies well. This is particularly striking for the reduced basis with only two elements, which gives an error of about 0.6% despite all ten parameters being varied in the test sample. In terms of speed-up when calculating the 500 testing points, the reduced basis with $n = 2$, 4, and 8 were 6, 4, and 2 times faster than the exact solver, respectively. We note that these speedups were obtained without precomputing any of the terms involved in Eqs. (3). Greater speed-ups can be achieved by precomputing as many of the terms in Eqs. (3) as possible, in the traditional strategy of an offline/online procedure often seen in RBM applications. Indeed, by separating the Hamiltonian in Eqs. (16) into the parts that can and cannot be precalculated (called affine and nonaffine in the RBM literature [19]), we achieve speed-ups of more than 250 times with respect to the exact solver for a reduced basis of two elements.

The parts of the Hamiltonian (16) that are nonaffine in the parameters can be made affine by using techniques such as the empirical interpolation method [64,65]. The terms that are nonlinear in the wave functions on the other hand, such as powers of the density ρ, can present a problem due to combinatorially increasing terms (M_k) in Eq. (4), a problem we plan to study further in a future work.

IV. CONCLUSIONS AND OUTLOOK

In this work, we have presented the reduced basis method as a useful framework for constructing emulators for general problems in nuclear physics, including nonlinear systems. We showcased the two steps of the process by first training a basis informed on high-fidelity solutions and then by obtaining the equations for the coefficients through the Galerkin projection. We discussed the connections of the eigenvector continuation literature with the RBM and showed that the emulators built through the former correspond to particular choices of the latter. We explained how the principal component analysis can be used to diagnose that a problem can be successfully emulated through the RBM and showcased the analysis on several examples. Finally, we applied the RBM to build an emulator for the nonlinear Gross-Pitaevskii equation and for the coupled nonlinear equations in Skyrme density functional theory. The built emulators showed excellent performance both for extrapolation and for speeding up computations, with a minimal loss in accuracy. Accurate extrapolation is important for systems with a large number of control parameters, and it is, therefore, not possible to fully cover the parameter space with training points. Extrapolation is also necessary for cases where the underlying computational methods break down for some range of the parameter space. Accurate emulators for speeding up calculations are crucial for real time evaluations, such as experimental design and control [66], and for multi-query evaluations, such as those involved in systematic studies and uncertainty quantification.

Within the DFT context, speed-up gains of more than 2 orders of magnitude will enable large-scale uncertainty quantification studies for a wide range of EDFs [67], an endeavor which, up to now, seemed inaccessible. Furthermore, the RBM approach could also reduce the penalty of using higher-dimensional solvers for systematic studies and uncertainty quantification, calculations previously limited to spherical and cylindrical symmetries. Finally, the trained emulators can be deployed in a cloud computing environment [68], fostering collaborative research, increasing the availability of cutting-edge research software, and improving scientific accessibility.

We hope our results help spark the interest of the nuclear theory community in RBMs. For this purpose, we created and will continue to update an online resource [69] to illustrate many of the concepts we discussed. The adoption of recent developments on the choice of ansatz subspaces [38,70,71], on error bounds and convergence properties [33,48,72], and

on the computational efficiency for nonaffine and nonlinear problems [64,65], to name a few, could become key in reaching the full extent of what these methods can offer. Given the simplicity and flexibility of the Galerkin projection and the PCA diagnostic we showcase to test for low-dimensional manifolds, we believe that RBMs have the potential to become standard tools for the emulation of challenging problems in many-body nuclear physics.

ACKNOWLEDGMENTS

We are very grateful to Witek Nazarewicz and Frederi Viens for their critical observations during the elaboration of this manuscript. We also thank Ana Posada, Jorge Piekarewicz, and Daniel Phillips for their careful read of the manuscript. This work was supported by the National Science Foundation CSSI program under Grant No. 2004601 (BAND Collaboration), the U.S. Department of Energy under Grant No. DOE-DE-NA0004074 (NNSA, the Stewardship Science Academic Alliances program), the U.S. Department of Energy (Grants No. DE-SC0013365 and No. DE-SC0021152), and the Nuclear Computational Low-Energy Initiative (NUCLEI) SciDAC-4 Project (Grant No. DE-SC0018083).

APPENDIX A: EQUIVALENCE OF THE REDUCED BASIS METHOD AND EIGENVECTOR CONTINUATION UNDER THE KOHN VARIATIONAL PRINCIPLE

As shown in the discussion, a direct application of the RBM to the scattering differential equation (5) leads to the following equations for the approximation coefficients:

$$\sum_{k=1}^{n} a_k \langle \phi_j - \phi_1 | F_\alpha(\phi_k) \rangle = 0, \quad \text{for} \quad j = 2, \ldots, n, \tag{A1}$$

and

$$a_1 = 1 - \sum_{k=2}^{n} a_k. \tag{A2}$$

We proceed to show the equivalence with the variational approach used in Refs. [13,15].

The (K-matrix) Kohn variational principle states that the solution to Eq. (5), with the asymptotic behavior (6), is a stationary point for the functional:

$$\beta[\phi] = \tau[\phi] - \int_0^\infty dr \phi(r) F_\alpha(\phi(r)), \tag{A3}$$

where $\tau[\phi]$ extracts its value from the asymptotic behavior of ϕ, that is, the cosine coefficient in Eq. (6).

The Kohn variational method is detailed in the Supplemental Material of Ref. [13]. It utilizes a trial function $\hat{\phi}_\alpha$ constructed exactly as in Eq. (7), and it finds a stationary point of the functional (A3) in terms of the coefficients a_k. After using the method of Lagrange multipliers to enforce the normalization condition, it is found that the following equation set describes the stationary point:

$$\tau_j - \lambda - \sum_{k=1}^{n} (\Delta U_{jk} + \Delta U_{kj}) a_k = 0 \quad \text{for} \quad j = 1, \ldots, n, \tag{A4}$$

where τ_j is the cosine coefficient in Eq. (6) associated with each ϕ_j, and the matrix ΔU_{jk} is a shorthand notation for the inner products:

$$\Delta U_{jk} = \langle \phi_j | F_\alpha(\phi_k) \rangle = \int_0^\infty dr \phi_j(r) F_\alpha(\phi_k(r)). \tag{A5}$$

These equations, together with the normalization condition $\sum_{k=1}^{n} a_k = 1$, can be used to find the n coefficients a_k plus the Lagrange multiplier λ.

Proof of equivalence between the methods

To compare Eq. (A4) to Eq. (A1), we need to rewrite Eq. (A4) in terms of ΔU_{jk} only, eliminating both τ_j and the Lagrange multiplier λ. We can relate the elements of ΔU_{kj} to their transposes ΔU_{jk} by integration by parts. Note that

$$-\int_0^\infty \phi_k \phi_j'' dr = -(\phi_k \phi_j' - \phi_k' \phi_j)\Big|_0^\infty - \int_0^\infty \phi_k'' \phi_j dr, \tag{A6}$$

where the boundary term can be evaluated through the boundary conditions (6) to be $\tau_j - \tau_k$. Therefore, via integration by parts, we can make F_α act on ϕ_j in Eq. (A5) to obtain

$$\Delta U_{kj} = \Delta U_{jk} + (\tau_j - \tau_k). \tag{A7}$$

Using this result we can eliminate ΔU_{kj} from Eq. (A4) and obtain

$$\tau_j - \lambda - \sum_{k=1}^{n} (2\Delta U_{jk}) a_k - \sum_{k=1}^{n} a_k (\tau_j - \tau_k) = 0$$

$$-\lambda - \sum_{k=1}^{n} (2\Delta U_{jk}) a_k + \sum_{k=1}^{n} a_k \tau_k = 0, \tag{A8}$$

for $j = 1, \ldots, n$, where we used the fact that the a_k sum to unity to cancel the τ_j term.

Next, we can eliminate the Lagrange multiplier λ and the sum of $a_k \tau_k$ by subtracting equations for different j. Without

TABLE II. Ranges for the 10 parameters used to generate the DFT results in Table I.

	Min	Max	Units
ρ_c	0.14	0.18	fm^{-3}
$E^{\mathrm{NM}}/\mathrm{A}$	−16.5	−14.5	MeV
K^{NM}	160	260	MeV
$a_{\mathrm{sym}}^{\mathrm{NM}}$	26	32	MeV
$L_{\mathrm{sym}}^{\mathrm{NM}}$	20	180	MeV
M_s^*	0.7	1.4	
$C_0^{\rho\Delta\rho}$	−55	−40	MeV fm^5
$C_1^{\rho\Delta\rho}$	−165	−90	MeV fm^5
$C_0^{\rho\nabla J}$	−105	−55	MeV fm^5
$C_1^{\rho\nabla J}$	−50	−15	MeV fm^5

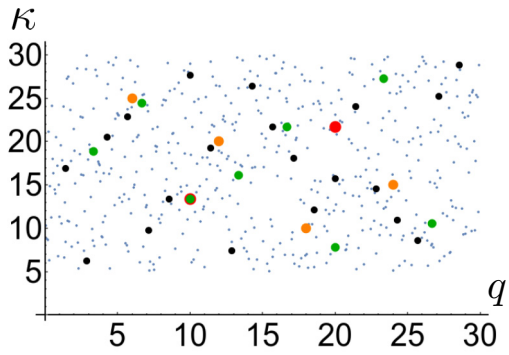

FIG. 4. Parameter values used for the results of the GP equation in Table I, all drawn by Latin hypercube sampling [47]. Points in blue show the 500 testing samples. Points in red, orange, and green show the parameters for the Lagrange RB built with two, four, and eight exact calculations, respectively. Points in black show the 20 parameters used to build the three POD RBs with $n = 2$, 4, and 8.

loss of generality, we can subtract all equations to the equation corresponding to $j = 1$, resulting in

$$\sum_{k=1}^{n}(\Delta U_{jk} - \Delta U_{1k})a_k = 0 \quad \text{for} \quad j = 2, \ldots, n. \tag{A9}$$

Finally, using the definition of $\Delta U_{jk} = \langle \phi_j | F_\alpha(\phi_k) \rangle$ shows the equivalence with Eq. (A1), completing the proof.

It is important to note that despite the equivalence in the approximation equations, variational techniques like Kohn's principle can have an improved accuracy on the calculations of certain quantities, such as τ. Indeed, the second term in Eq. (6) can be thought as a first-order correction to τ through a factor proportional to the residual $F_\alpha(\hat{\phi}_\alpha)$. Therefore, when implementing a RBM emulator, even if we choose the basis ϕ or the projecting functions ψ in a way that we do not recover the same equations for the coefficients as a variational principle, it could be beneficial to include the associated correction terms to help increase accuracy.

APPENDIX B: DETAILS ABOUT THE NUMERICAL RESULTS

The codes used to generate all the results we presented can be found in Ref. [73].

1. Decay of singular values

In this section, we give details on the construction of the singular values σ_k from the singular value decomposition (SVD) shown in Figs. 1 and 2 in Sec. II B. Four problems were considered: the infinite well (IW), the single-channel two-body scattering with a Minnesota potential at fixed energy (SME) and varying energy (SME^*), the Gross-Pitaevskii equation (GP), and ^{48}Ca under density functional theory (DFT).

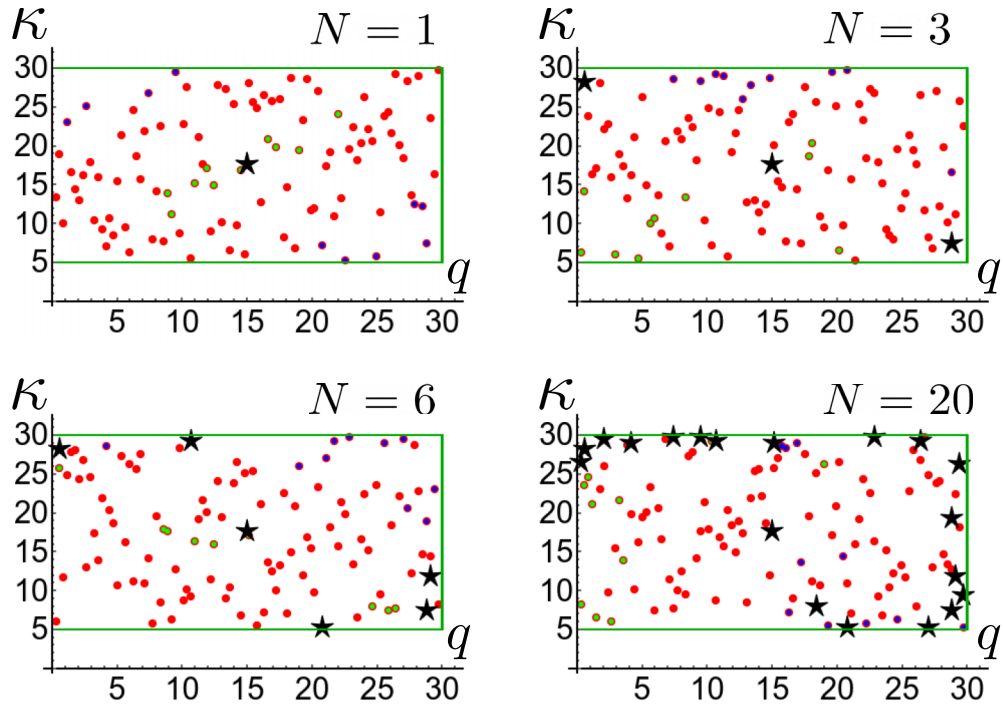

FIG. 5. Construction of the POD + Greedy RB for the results in Table I. The black stars show the N exact calculations made at each stage to build the POD + Greedy basis. The four panels show the stages for $N = 1$, 3, 6, and 20. The red points in each panel are the 100 LHS draws on which the norm of the residual is maximized each time to add a new exact calculation to the POD + Greedy RB. This random sampling is repeated on each step (no two panels share the same red points). Points in blue and green on each panel show the ten locations where the residual is maximized or minimized, representing the regions where the emulator is performing poorly and adequately, respectively. The green box shows the limits for the LHS: $q \in [0, 30]$ and $\kappa \in [5, 30]$.

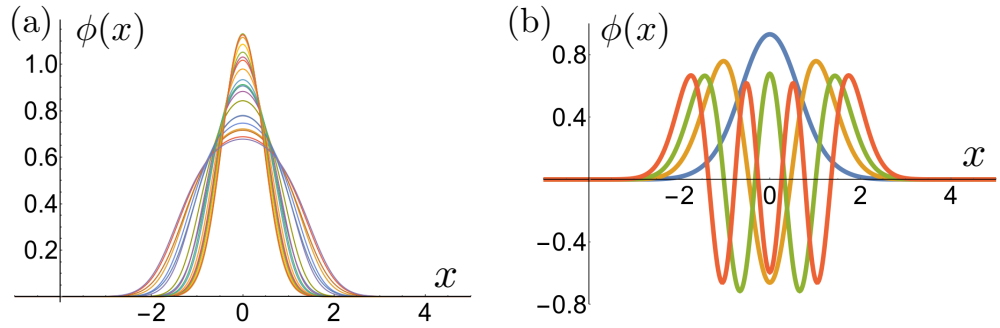

FIG. 6. Panel (a) shows the 20 exact solutions $\phi_{q,\kappa}(x)$ obtained by the Greedy algorithm in Fig. 5 and used to construct the POD + Greedy basis for the results of Table I. Panel (b) shows the first four principal components of this set, which constitute the RB used for the POD + Greedy results with $n = 4$ in Table I.

The infinite well problem consists of the 1D quantum Hamiltonian of a particle trapped in an infinite well (IW) [39] where α controls the location of the well:

$$V(x,\alpha) = \begin{cases} 0, & \alpha < x < \alpha + 1, \\ \infty, & \text{otherwise.} \end{cases} \tag{B1}$$

The ground-state solutions to this Hamiltonian are wave functions of the form $\phi_\alpha = \sqrt{2}\sin[\pi(x-\alpha)]$ for $\alpha < x < \alpha + 1$ and zero otherwise. The singular values σ_k for the IW showed in Fig. 1 were obtained by sampling 40 values of α in the range $[-5, 5]$ using Latin hypercube sampling (LHS) and performing SVD on the set of 40 solutions.

Both SME and SME^* problems consist of the single-channel $^1S_0$ nucleon-nucleon scattering Hamiltonian [28]. The Minnesota potential $V(r,\alpha)$ [37], with parameters $\alpha = V_{0R}$ and V_{0S}, is used for the interaction, while the two nonlinear parameters associated with the Gaussian's widths remained fixed. In both cases, we make the change of variables $s = pr$ and the scattering Hamiltonian takes the form

$$\left(-\frac{d^2}{ds^2} + \frac{\ell(\ell+1)}{s^2} + \tilde{U}(s,\alpha,p) - 1\right)\phi_\alpha(s) = 0, \tag{B2}$$

where the potential $\tilde{U}(s,\alpha,p) = V(s/p,\alpha)2\mu/p^2$ is now momentum dependent. In both cases (SME and SME^*), 40 parameters where obtained by a LHS in the range $V_{0R} = [100, 300]$ MeV and $V_{0S} = [-200, 0]$ MeV, following Ref. [13]. The singular values showed in Fig. 1 were obtained by performing SVD on the set of 40 solutions. In the case of SME, all 40 solutions shared the same energy in the center of mass $E = 50$ MeV, while for SME^* the energies where equispaced in the range $E = [20, 80]$ MeV.

The GP and DFT cases are explained in detail in Sec. III. The ranges for the parameters in both cases correspond to the ones used in Table I. For GP, a set of 40 values of the parameters $[q,\kappa]$ were obtained by LHS in the range $q \in [0, 30]$ and $\kappa \in [5, 30]$. For DFT, 50 values of the parameters were obtained with a LHS across the parameter ranges shown in Table II.

2. One-dimensional Gross-Pitaevskii equation with a harmonic trapping potential

The four training points ϕ_k used in the Lagrange basis for the results in Fig. 3(a) are $[q,\kappa] = \{[0, 1], [0, 5], [0.5, 1], [0.5, 5]\}$. Figure 4 shows the training points for the Lagrange and POD RB, as well as the 500 testing points used for the results shown in Table I. Figure 5 shows the construction on the POD + Greedy basis also used for the results shown in Table I. Figure 6 shows the 20 exact solutions $\phi_{q,\kappa}(x)$ selected by the Greedy algorithm, as well as the first four principal components of this set.

Description of the POD + Greedy scheme used for GP

The POD + Greedy scheme used for the results of Table I consists of iteratively constructing a set of N exact solutions (ES) with a (weak) Greedy algorithm [19] informed by the residuals of a POD RB of dimension n_2 derived from the set of exact solutions at each step. To set up the algorithm, let $POD(\{\tilde{\phi}_l\}_{l=1}^N, n)$ be a function that returns a normalized basis constructed with first n principal components of the set of solutions $\{\tilde{\phi}_l\}_{l=1}^N$ if $N \geqslant n$ and that returns $POD(\{\tilde{\phi}_l\}_{l=1}^N, N)$ if $N < n$. This function can be used to construct a POD basis of size up to n with a set of solutions. The Greedy strategy we used is summarized in Algorithm 1. The desired POD bases were constructed by running $POD(RB, n)$ on the output of this algorithm with $\alpha_1 = [q_1, \kappa_1] = [15, 17.5]$, $n_2 = 10$, $N = 20$, and $N_2 = 100$.

Algorithm 1: POD + Greedy scheme

Define starting parameters α_1, n_2, N, N_2
Find $\tilde{\phi}_1$ s.t. $F_{\alpha_1}(\tilde{\phi}_1) = 0$
$ES \leftarrow \{\tilde{\phi}_1\}$
For $i = 2, \ldots, N$ **do**
$RB \leftarrow POD(ES, n_2)$
Draw N_2 parameters with LHS: $A = \{\hat{\alpha}_1, \ldots, \hat{\alpha}_{N_2}\}$
Use the RBM with the RB to find $\hat{\phi}_{\hat{\alpha}}$ for each element in A
$\alpha_i \leftarrow \arg\max_{\hat{\alpha}\in A} ||F_{\hat{\alpha}}(\hat{\phi}_{\hat{\alpha}})||^2$
Find $\tilde{\phi}_i$ s.t. $F_{\alpha_i}(\tilde{\phi}_i) = 0$
$ES \leftarrow ES \cup \{\tilde{\phi}_i\}$
end
return ES

TABLE III. Glossary of acronyms.

Acronym	Name	Brief description	Detailed Ref.
EC	Eigenvector continuation	Numerical method for approximating the "trajectory" of an eigenvector associated with a parametrized operator as the corresponding parameters change. As shown in this article, it can be seen as a special case of the RBM.	[11,74]
RBM	Reduced basis method	Numerical method for solving parametrized differential equations efficiently by using a handful of previously computed solutions.	Chap. 3 in [19,20]
SVD	Singular value decomposition	Matrix factorization algorithm key for many modern computational methods, including PCA and POD.	Chap. 1 in [22], Chap. 2 in [75]
POD	Proper orthogonal decomposition	SVD application to partial differential equations used to capture a low-dimensional representation of the corresponding dynamical system. In the context of RBMs it is used to construct small bases that capture a low-dimensional representation of a larger set of "exact" solutions.	Sec. 3.3.1 in [20], Chap. 6 in [19], Sec. 11.1 in [22]
PCA	Principal component analysis	SVD application where the variability of high-dimensional data is decomposed into its more statistically descriptive factors.	Chap. 1 in [22], [76–78]
LHS	Latin hypercube sampling	Sampling technique for efficiently distributing points in $\mathbb{R}^n$.	[47]
	Greedy algorithm	Algorithm that selects the locally optimal choice on each iteration. In the context of RBMs, it sequentially selects "exact" solutions to train the emulator, usually by maximizing an estimated error.	Sec. 3.2.2 in [20], Chap. 7 in [19], [50]
	Lagrange basis	A reduced basis of size n for the RBM that is built as a linear combination of only n "exact" solutions.	[24]
DFT	Density functional theory	Mean-field approach to many-body quantum systems.	[51,79]
EDF	Energy density functional	The object that defines the interaction used in DFT.	[51,79]

3. Nuclear density functional theory

The four training points, ϕ_k, used in Fig. 3(b) only varied the $K^{\rm NM}$ and $L_{\rm sym}^{\rm NM}$ parameters, with the rest taken to be the standard UNEDF1 optimal parameters [62]. The four values of $K^{\rm NM}$ and $L_{\rm sym}^{\rm NM}$, in MeV, are

$$K^{\rm NM}=200,\ L_{\rm sym}^{\rm NM}=30;\quad K^{\rm NM}=200,\ L_{\rm sym}^{\rm NM}=60;$$
$$K^{\rm NM}=220,\ L_{\rm sym}^{\rm NM}=30;\quad K^{\rm NM}=220,\ L_{\rm sym}^{\rm NM}=60.$$

Table II shows the parameter ranges used for the LHS for the DFT results in Table I. Both the 500 testing points and the $N=20$ exact evaluations used to build the POD RB were independently drawn by LHS on these ranges.

APPENDIX C: GLOSSARY OF TERMINOLOGY

Table III shows the frequently used terms in this work (inspired by Ref. [80]).

[1] D. R. Phillips, R. J. Furnstahl, U. Heinz, T. Maiti, W. Nazarewicz, F. M. Nunes, M. Plumlee, M. T. Pratola, S. Pratt, F. G. Viens, and S. M. Wild, J. Phys. G: Nucl. Part. Phys. **48**, 072001 (2021).

[2] A. Ekström, C. Forssén, C. Dimitrakakis, D. Dubhashi, H. T. Johansson, A. S. Muhammad, H. Salomonsson, and A. Schliep, J. Phys. G: Nucl. Part. Phys. **46**, 095101 (2019).

[3] J. Melendez, R. Furnstahl, H. Grießhammer, J. McGovern, D. Phillips, and M. Pratola, Eur. Phys. J. A **57**, 1 (2021).

[4] P. G. Giuliani and J. Piekarewicz, Phys. Rev. C **104**, 024301 (2021).

[5] S. Pratt, E. Sangaline, P. Sorensen, and H. Wang, Phys. Rev. Lett. **114**, 202301 (2015).

[6] J. D. McDonnell, N. Schunck, D. Higdon, J. Sarich, S. M. Wild, and W. Nazarewicz, Phys. Rev. Lett. **114**, 122501 (2015).

[7] S. Wesolowski, R. Furnstahl, J. Melendez, and D. Phillips, J. Phys. G: Nucl. Part. Phys. **46**, 045102 (2019).

[8] R.-D. Lasseri, D. Regnier, J.-P. Ebran, and A. Penon, Phys. Rev. Lett. **124**, 162502 (2020).

[9] K. Godbey, A. S. Umar, and C. Simenel, arXiv:2206.04150.

[10] T. J. Santner, B. J. Williams, W. I. Notz, and B. J. Williams, *The Design and Analysis of Computer Experiments* (Springer, New York, 2003), Vol. 1, https://doi.org/10.1007/978-1-4757-3799-8.

[11] D. Frame, R. He, I. Ipsen, D. Lee, D. Lee, and E. Rrapaj, Phys. Rev. Lett. **121**, 032501 (2018).

[12] S. König, A. Ekström, K. Hebeler, D. Lee, and A. Schwenk, Phys. Lett. B **810**, 135814 (2020).

[13] R. Furnstahl, A. Garcia, P. Millican, and X. Zhang, Phys. Lett. B **809**, 135719 (2020).

[14] J. Melendez, C. Drischler, A. Garcia, R. Furnstahl, and X. Zhang, Phys. Lett. B **821**, 136608 (2021).

[15] C. Drischler, M. Quinonez, P. Giuliani, A. Lovell, and F. Nunes, Phys. Lett. B **823**, 136777 (2021).

[16] C. Cohen-Tannoudji, B. Diu, and F. Laloe, *Quantum Mechanics* (Wiley & Sons, New York, 1986), Vol. 2.

[17] W. Kohn, Phys. Rev. **74**, 1763 (1948).

[18] B. O. Almroth, P. Stern, and F. A. Brogan, AIAA J. **16**, 525 (1978).

[19] A. Quarteroni, A. Manzoni, and F. Negri, *Reduced Basis Methods for Partial Differential Equations: An Introduction*, UNITEXT - La Matematica per il 3+2 Vol. 92 (Springer, Cham, 2015), https://doi.org/10.1007/978-3-319-15431-2.

[20] J. S. Hesthaven, G. Rozza, B. Stamm *et al.*, *Certified Reduced Basis Methods for Parametrized Partial Differential Equations*, Springer Briefs in Mathematics Vol. 590 (Springer, Cham, 2016), https://doi.org/10.1007/978-3-319-22470-1.

[21] A. Quarteroni, G. Rozza *et al.*, *Reduced Order Methods for Modeling and Computational Reduction*, Modeling, Simulation & Applications Vol. 9 (Springer, Cham, 2014), https://doi.org/10.1007/978-3-319-02090-7.

[22] S. L. Brunton and J. N. Kutz, *Data-Driven Science and Engineering: Machine Learning, Dynamical Systems, and Control* (Cambridge University, Cambridge, England, 2019), https://doi.org/10.1017/9781108380690.

[23] J. A. Melendez, C. Drischler, R. Furnstahl, A. Garcia, and X. Zhang, J. Phys. G: Nucl. Part. Phys. **49**, 102001 (2022).

[24] A. Quarteroni, G. Rozza, and A. Manzoni, J. Math. Ind. **1**, 3 (2011).

[25] N. C. Nguyen, G. Rozza, D. B. P. Huynh, and A. T. Patera, *Large-Scale Inverse Problems and Quantification of Uncertainty* (Wiley & Sons, New York, 2010), Chap. 8, pp. 151–177, https://doi.org/10.1002/9780470685853.ch8.

[26] S. E. Field, C. R. Galley, F. Herrmann, J. S. Hesthaven, E. Ochsner, and M. Tiglio, Phys. Rev. Lett. **106**, 221102 (2011).

[27] R. Milani, A. Quarteroni, and G. Rozza, Comput. Methods Appl. Mech. Eng. **197**, 4812 (2008).

[28] I. J. Thompson and F. M. Nunes, *Nuclear Reactions for Astrophysics: Principles, Calculation and Applications of Low-Energy Reactions* (Cambridge University, Cambridge, England, 2009), https://doi.org/10.1017/CBO9781139152150.

[29] I. T. Jolliffe, *Principal Component Analysis* (Springer, New York, 2002), https://doi.org/10.1007/b98835.

[30] A. Blum, J. Hopcroft, and R. Kannan, *Foundations of Data Science* (Cambridge University, Cambridge, England, 2020), https://doi.org/10.1017/9781108755528.

[31] G. Rawitscher, V. dos Santos Filho, and T. C. Peixoto, *An Introductory Guide to Computational Methods for the Solution of Physics Problems* (Springer, Cham, 2018), pp. 17–31, https://doi.org/10.1007/978-3-319-42703-4.

[32] C. A. J. Fletcher, *Computational Galerkin Methods* (Springer, New York, 1984), https://doi.org/10.1007/978-3-642-85949-6.

[33] A. Buffa, Y. Maday, A. T. Patera, C. Prud'homme, and G. Turinici, ESAIM: Math. Model. Numer. Anal. **46**, 595 (2012).

[34] C. Prud'homme, D. V. Rovas, K. Veroy, L. Machiels, Y. Maday, A. T. Patera, and G. Turinici, J. Fluids Eng. **124**, 70 (2002).

[35] R. R. Lucchese, Phys. Rev. A **40**, 6879 (1989).

[36] S. Singh and A. Stauffer, Nuovo Cimento B **22**, 139 (1974).

[37] D. Thompson, M. LeMere, and Y. Tang, Nucl. Phys. A **286**, 53 (1977).

[38] M. Nonino, F. Ballarin, G. Rozza, and Y. Maday, arXiv:1911.06598.

[39] C. Cohen-Tannoudji, B. Diu, and F. Laloe, *Quantum Mechanics* (Wiley & Sons, New York, 1986), Vol. 1.

[40] E. P. Gross, Nuovo Cimento **20**, 454 (1961).

[41] L. P. Pitaevskii, J. Exp. Theor. Phys. **13**, 451 (1961).

[42] F. Pichi, A. Quaini, and G. Rozza, SIAM J. Sci. Comput. **42**, B1115 (2020).

[43] L. D. Carr, C. W. Clark, and W. P. Reinhardt, Phys. Rev. A **62**, 063610 (2000).

[44] L. D. Carr, C. W. Clark, and W. P. Reinhardt, Phys. Rev. A **62**, 063611 (2000).

[45] L. D. Carr, C. W. Clark, and W. P. Reinhardt, Int. J. Mod. Phys. B **15**, 1663 (2001).

[46] G. Torres-Vega, J. Phys.: Conf. Ser. **792**, 012054 (2017).

[47] M. D. Mckay, R. J. Beckman, and W. J. Conover, Technometrics **42**, 55 (2000).

[48] K. Veroy, C. Prud'Homme, D. Rovas, and A. Patera, *16th AIAA Computational Fluid Dynamics Conference* (American Institute of Aeronautics & Astronautics, Reston, VA, 2003), p. 3847.

[49] B. Haasdonk and M. Ohlberger, ESAIM: M2AN **42**, 277 (2008).

[50] A. Sarkar and D. Lee, Phys. Rev. Res. **4**, 023214 (2022).

[51] *Energy Density Functional Methods for Atomic Nuclei*, edited by N. Schunck (IOP, Bristol, England, 2019), https://doi.org/10.1088/2053-2563/aae0ed.

[52] É. Cancès, C. L. Bris, Y. Maday, N. Nguyen, A. Patera, and G. Pau, *CRM Proceedings and Lecture Notes* (American Mathematical Society, Providence, 2007), pp. 15–47, https://doi.org/10.1090/crmp/041.

[53] L. Lin, J. Lu, L. Ying, and E. Weinan, J. Comput. Phys. **231**, 2140 (2012).

[54] G. Zhang, L. Lin, W. Hu, C. Yang, and J. E. Pask, J. Comput. Phys. **335**, 426 (2017).

[55] T. H. R. Skyrme, Philos. Mag. **1**, 1043 (1956).

[56] T. Skyrme, Nucl. Phys. **9**, 615 (1958).

[57] D. Vautherin and D. M. Brink, Phys. Rev. C **5**, 626 (1972).

[58] Y. Engel, D. Brink, K. Goeke, S. Krieger, and D. Vautherin, Nucl. Phys. A **249**, 215 (1975).

[59] J. Dobaczewski and J. Dudek, Phys. Rev. C **52**, 1827 (1995).

[60] E. Chabanat, P. Bonche, P. Haensel, J. Meyer, and R. Schaeffer, Nucl. Phys. A **627**, 710 (1997).

[61] M. Kortelainen, T. Lesinski, J. Moré, W. Nazarewicz, J. Sarich, N. Schunck, M. V. Stoitsov, and S. Wild, Phys. Rev. C **82**, 024313 (2010).

[62] M. Kortelainen, J. McDonnell, W. Nazarewicz, P.-G. Reinhard, J. Sarich, N. Schunck, M. V. Stoitsov, and S. M. Wild, Phys. Rev. C **85**, 024304 (2012).

[63] G. Hagen, A. Ekström, C. Forssén, G. Jansen, W. Nazarewicz, T. Papenbrock, K. Wendt, S. Bacca, N. Barnea, B. Carlsson *et al.*, Nat. Phys. **12**, 186 (2016).

[64] M. Barrault, Y. Maday, N. C. Nguyen, and A. T. Patera, C. R. Math. **339**, 667 (2004).

[65] M. A. Grepl, Y. Maday, N. C. Nguyen, and A. T. Patera, ESAIM: Math. Modell. Numer. Anal. **41**, 575 (2007).

[66] S. A. Miskovich, F. Montes, G. P. A. Berg, J. Blackmon, K. A. Chipps, M. Couder, C. M. Deibel, K. Hermansen, A. A. Hood, R. Jain, T. Ruland, H. Schatz, M. S. Smith, P. Tsintari, and L. Wagner, Phys. Rev. Accel. Beams **25**, 044601 (2022).

[67] P. Giuliani, K. Godbey, E. Bonilla, F. Viens, and J. Piekarewicz, arXiv:2209.13039.

[68] K. Godbey and P. Giuliani, BMEX, Bayesian Mass Explorer (2022), https://bmex.dev/.
[69] K. Godbey, P. Giuliani, E. Bonilla, E. Flynn, R. Garg, and D. Odell, Introduction to reduced-basis methods in nuclear physics, https://kylegodbey.github.io/nuclear-rbm/.
[70] P. Benner, S. Gugercin, and K. Willcox, SIAM Rev. **57**, 483 (2015).
[71] M. Ohlberger and S. Rave, C. R. Math. **351**, 901 (2013).
[72] A. Cohen, W. Dahmen, R. DeVore, and J. Nichols, ESAIM: M2AN **54**, 1509 (2020).
[73] https://github.com/kylegodbey/nuclear-rbm/tree/paperarchive.
[74] A. Sarkar and D. Lee, Phys. Rev. Lett. **126**, 032501 (2021).
[75] G. H. Golub and C. F. Van Loan, *Matrix Computations* (John Hopkins University, Baltimore, 2013).
[76] H. Hotelling, J. Educ. Psychol. **24**, 417 (1933).
[77] M. Turk and A. Pentland, J. Cognit. Neurosci. **3**, 71 (1991).
[78] I. T. Jolliffe and J. Cadima, Philos. Trans. R. Soc. A **374**, 20150202 (2016).
[79] M. Bender, P.-H. Heenen, and P.-G. Reinhard, Rev. Mod. Phys. **75**, 121 (2003).
[80] P. Bedaque, A. Boehnlein, M. Cromaz, M. Diefenthaler, L. Elouadrhiri, T. Horn, M. Kuchera, D. Lawrence, D. Lee, S. Lidia *et al.*, Eur. Phys. J. A **57**, 100 (2021).